Reliability analysis of riverbank stability accounting for the intrinsic variability of unsaturated soil parameters

*Article Title:*

# Reliability analysis of riverbank stability accounting for the intrinsic variability of unsaturated soil parameters

*Journal Name:*

**Structural Safety**

*Authors:*

**Guido Gottardi[a,*], Carmine G. Gragnano[b], Marco Ranalli[c], Laura Tonni[d]**

[a,*]*Corresponding Author, Department of Civil, Chemical, Environmental and Materials Engineering, DICAM, Alma Mater Studiorum - University of Bologna.* Viale Risorgimento 2, 40136 Bologna (Italy). Phone: +39 0512093524.
E-mail: guido.gottardi2@unibo.it

[b]*Department of Civil, Chemical, Environmental and Materials Engineering, DICAM, Alma Mater Studiorum - University of Bologna.* Viale Risorgimento 2, 40136 Bologna (Italy).
E-mail: carmine.gragnano2@unibo.it

[c]*Department of Civil, Chemical, Environmental and Materials Engineering, DICAM, Alma Mater Studiorum - University of Bologna.* Viale Risorgimento 2, 40136 Bologna (Italy).
E-mail: marco.ranalli@unibo.it

[d]*Department of Civil, Chemical, Environmental and Materials Engineering, DICAM, Alma Mater Studiorum - University of Bologna.* Viale Risorgimento 2, 40136 Bologna (Italy).
E-mail: laura.tonni@unibo.it
ORCID 0000-0002-9391-6661

# Abstract

The paper presents a probabilistic study aimed at investigating the role of the soil hydraulic response on the stability of existing river embankments, for which the uncertainty and the inherent variability of geotechnical and hydraulic properties are typically greater when compared to new flood defence structures. The study has been carried out with reference to a specific, thoroughly investigated 20 m-long segment of the river Secchia banks (northern Italy), which experienced a catastrophic sudden failure after a period of intense rainfall, in January 2014. By taking such well-documented case as a base, the proposed probabilistic analyses consider three key aspects, typically disregarded in routine risk assessment procedures: i) transient seepage flow through earth structures due to time dependent hydraulic loads, ii) unsaturated conditions of soils forming the river embankment, iii) uncertainty of the soil model parameters, with special emphasis placed on the impact of intrinsic variability of unsaturated soil parameters. The numerical results, obtained from the application of the *Point Estimate Method*, allow identifying the crucial role of suction distribution on the probability of failure of the riverbank slopes and clearly show that such probability can be significantly underestimated when the variability of hydraulic parameters is neglected.



**Keywords:** unsaturated soil, transient seepage, probabilistic analysis, Point Estimate Method, riverbank stability

# 1. Introduction

The evaluation of riverbank stability represents a fundamental task in georisk assessment. Indeed, overestimating the safety margin of a flood defence structure may potentially lead to totally unexpected failures and subsequent severe consequences in terms of damages, repairing costs and human losses. Hence, a thorough understanding of the different factors adversely affecting riverbank stability and the way they interact to determine failure conditions is a necessary step for engineers in order to design successful and cost-effective countermeasures against potential collapses.

In recent years, the use of numerical methods has offered a powerful means to develop accurate groundwater seepage models, enabling transient analyses coupled with unsaturated stress approaches for the evaluation of the dynamic distribution of pore water pressure due to rainfall events, evaporation and river level fluctuations. A number of studies ([1-2] among others), based on different numerical approaches, have thus investigated in great detail the effect of changes in pore water pressures on the riverbank stability, with special attention paid to the crucial role of matric suction and its influence on the soil properties in the partially saturated zone of the embankment.

At the same time, numerical analysis has proved to be a suitable and effective tool in order to take into account a further fundamental geotechnical issue, that is the intrinsic variability of soils properties, even in relatively homogeneous deposits, together with the unavoidable uncertainties due to limited experimental data and to the related correlation models adopted for soil characterization [3-8].

A large number of research contributions (e.g. [9-14]), based on either theoretical applications or failure case studies, have discussed the effect of uncertainties and spatial variation of soil shear strength on slope analysis reliability, whilst only few available studies have also considered the variability of hydraulic properties, particularly those governing the behaviour of unsaturated soils [15-16]. An even more limited number of published works [17] have actually tackled the problem with reference to existing river embankments and a substantial lack of applications to relevant case

studies is thus observed. However, in these structures the spatial variability of hydraulic properties, especially in unsaturated soil conditions, may remarkably affect both the seepage regime [18-19], which results in specific flow paths, and the unsaturated soil shear strength [20], with significant implications on the overall stability.

In order to gain a better insight into such geotechnical issues, this paper presents an extensive probabilistic study specifically aimed at investigating the role of the intrinsic variability of unsaturated soil hydraulic properties in the assessment of existing riverbank safety conditions. The study has been carried out using the geotechnical dataset collected along a 20 m bank segment of the Secchia river, a right tributary of the major Po river, north of the historic town of Modena (Italy). Following the catastrophic failure occurred in January 2014 [21], this river embankment segment was thoroughly investigated by means of in situ and laboratory tests and a valuable and varied database has thus become available for the analyses. Starting from such well-documented real case, the objective of the study is primarily to examine the effect of different geotechnical sources of uncertainties on riverbank stability, with specific emphasis on the crucial impact of intrinsic variability of unsaturated soil hydraulic parameters. After a brief summary of the *Point Estimate Method* (PEM), which is the probabilistic approach adopted in this numerical study, and of the accurate geotechnical characterization of the sediments forming the whole river embankment system, the paper first presents the results of a few preliminary limit equilibrium analyses under steady-state seepage conditions, assuming soil shear strength as the only source of uncertainty. Next, two further series of limit equilibrium analyses, performed under transient flow conditions as induced by fluctuating river levels and rainfall events, are shown and the effect of assuming hydraulic parameters either as deterministic or random variables is discussed with respect to the resulting probability of riverbank failure. As regards the specific collapse that led to the January 2014 large breach in the Secchia river embankment, it is worth observing that in such case the triggering mechanism was eventually ascribed to a potential local lack of structural integrity induced by animal burrows [21], which is outside the scope of this study and therefore it will not be

72 considered in the following analyses. However, the localised damages observed in the surroundings
73 of the failed section, coupled with the reduction in saturation degree and suction caused by
74 persistent and ever increasing high water events, have shown the need to further explore the actual
75 factors affecting the potential riverbank instability and to provide a rational methodological
76 approach to take into account the unavoidable intrinsic variability of the soil parameters which
77 control the local conditions.
78

79 ## 2. Uncertainty propagation methods

80 The uncertainty propagation analysis allows propagating the errors from input data (e.g. mechanical
81 properties, retention and hydraulic soil parameters) to the final result (i.e. the factor of safety and
82 the probability of failure in ultimate limit state analyses). In geotechnical practice and research, a
83 number of simplified uncertainty propagation methods, like *First Order Second Moment Method*
84 (FOSM), *Point Estimate Method* (PEM) or *First Order Reliability Method* (FORM) have long been
85 successfully adopted (e.g. [9,22-25]). Such approaches are often used as a valid alternative to more
86 accurate and well-established procedures, typically the *Monte Carlo Method* (MCM), which turn
87 out to be more difficult to be implemented and very time-consuming when adopted in slope stability
88 analyses based on Limit Equilibrium or Finite Element methods [25]. In addition to the simplified
89 FOSM, PEM and FORM mentioned above, in recent years advanced stochastic approaches, capable
90 of combining accuracy with computational efficiency, have been also proposed in the literature with
91 the aim of overcoming the prohibitive time and resources efforts required by the direct MCM.
92 Among them, it is worth mentioning the *Stochastic Response Surface Method* [26] and, in
93 particular, the *Subset Simulation* [27-29]. However, although these latest computational strategies
94 have been devised to alleviate and facilitate the application of probability-based approaches in slope
95 assessment, their use in routine engineering practice is still far from being widespread, probably due
96 to complexity of the relevant implementation algorithms. Some authors (e.g. [28]) also observed
97 that *Subset Simulation* still requires a significant computational cost at extremely small probability

98 levels (e.g., probability of failure $P_f$ <$10^{-4}$~$10^{-5}$).

99 At the same time the simplified methods, though approximated, appear to provide a valid, efficient
100 and relatively easy tool to incorporate spatial variability of soil properties into reliability analysis
101 and risk assessment of slope stability, especially when failure probability is not very low. In this
102 case, indeed, such methods typically result in an approximate but not erroneous estimate of the
103 probability of failure. Regarding this point, it is worth observing also that the accuracy of the
104 computed probability of failure largely depends on the reliability of the statistical characterization
105 of the input parameters, and that the estimates of the probability of failure should be interpreted in
106 terms of their order of magnitude, as emphasized by Duncan and Sleep [30].

107 In this work, the *Point Estimate Method* in particular was used as probabilistic procedure to
108 propagate the uncertainty from the geotechnical and hydraulic soil properties to the probability of
109 failure ($P_f$) of the riverbank slopes. Computational efficiency, together with a rather straightforward
110 implementation procedure, caused PEM to be selected instead of MCM. In spite of a certain
111 "roughness" of the adopted method, a few preliminary analyses, carried out with both PEM and
112 MCM and accounting for the only uncertainties on soil shear strength, led to numerically different
113 results, lying however in the same order of magnitude. This outcome, obtained for values of $P_f$
114 relatively high, cannot be obviously considered as generally valid.

115 The *Point Estimate Method* is widely used when no closed-form analytical solutions are available
116 and a number of successful applications of the method [31-33] to typical geotechnical stability
117 problems, either using Limit Equilibrium Method (LEM) or the Finite Element Method (FEM), can
118 be found in the literature. Furthermore, in recent years the PEM has been implemented in a number
119 of commercial codes that are commonly used for stability analyses, hence its use is very likely to
120 earn popularity among engineers also for routine applications.

121

122 ## 2.1 Adopted probabilistic approach

123 The *Point Estimate Method* consists in replacing the continuous random variables, characterized by
124 a probability density function, with discrete random variables described by two or more points with
125 assigned weight. The discrete points and the relevant weights are estimated on the basis of the
126 statistical moments of the continuous random variables, i.e. mean value, variance and skewness
127 coefficient.
128 The original PEM [34-36] allowed considering such first three statistical moments only in case of
129 function of a single random variable; in case of multiple variables, the application of the method
130 was restricted to systems of correlated and symmetrically distributed random variables. The later
131 formulation developed by Panchalingam and Harr [37] allowed incorporating both correlated and
132 skewed random variables into the uncertainty analysis in the case of multivariate random variables
133 problems as well. The key features of the method are briefly summarized below.
134 Let $f(X) = f(X_1, X_2, \ldots, X_N)$ be a function of $N$ correlated and skewed random variables. The first
135 three statistical moments (mean, standard deviation and skewness coefficient) and the correlation
136 structure of random variables are assumed to be known.
137 The method firstly defines the point estimate locations through the statistical moments of the
138 random variables. For each random variable, two point estimate locations are evaluated, according
139 to the following relationships:

140 (1) $$X_+ = \mu_X + \left[\frac{\nu_X}{2} + \sqrt{1 + \left(\frac{\nu_X}{2}\right)^2}\right]\sigma_X$$

141 (2) $$X_- = \mu_X + \left[\frac{\nu_X}{2} - \sqrt{1 + \left(\frac{\nu_X}{2}\right)^2}\right]\sigma_X$$

142 where $\mu_X$ is the mean value, $\sigma_X$ is the standard deviation and $\nu_X$ is the skewness coefficient.
143 Estimate locations $X_+$ and $X_-$ are then associated with weights $P_+$ and $P_-$ respectively. These are
144 given by:

145 (3) $$P_+ = \frac{1}{2}\left[1 - \frac{\nu_X}{2}\frac{1}{\sqrt{1+(\nu_X/2)^2}}\right]$$

146 (4) $$P_- = 1 - P_+$$

For a function of $N$ random variables, the method provides $2^N$ point estimate locations, resulting from all possible combinations of point estimate locations. Accordingly, the weight associated with a general combination ($X_{1\pm}$, $X_{2\pm}$, ..., $X_{N\pm}$) is defined as:

(5) $$P_{\pm\pm\cdots\pm} = P_{1\pm}P_{2\pm}\ldots P_{N\pm} + \sum_{i=1}^{N-1}\sum_{j=i+1}^{N}(\pm)_i(\pm)_j a_{ij}P_{ij}$$

where $a_{ij} = \rho_{ij}\,(P_{i+}P_{i-}P_{j+}P_{j-})^{0.5}$, $\rho_{ij}$ = correlation coefficient between the random variables $X_i$ and $X_j$, $P_{ij} = P_{1\pm}P_{2\pm}\ldots P_{k\pm}\ldots P_{N\pm}$ ($k \neq i$ and $k \neq j$).

The statistical m-th moment of the function $f(X)$ can be therefore expressed as follows:

(6) $$E[f(x)^m] \approx \sum_{j=1}^{k} P_j f\left(X_j\right)^m$$

where $k$ is the number of point estimate locations, $P_j$ is the weight associated with combination $j$, $f(X_j)$ is the function evaluated at point estimate location $j$. In particular, the mean $\mu_{f(X)}$ and the variance $\sigma^2_{f(X)}$ of the function can be then estimated according to the following relationships:

(7) $$\mu_{f(X)} = E[f(x)]$$

(8) $$\sigma^2_{f(X)} = E[f(X)^2] - (E[f(x)])^2$$

Finally, the reliability index $\beta$ and the probability of failure $P_f$ are given by:

(9) $$\beta = \frac{\mu_{SF}-1}{\sigma_{SF}}$$

(10) $$P_f = 1 - \Phi(\beta)$$

where $\Phi$ is the cumulative distribution of the standard normal random variable. A Normal probability distribution of the safety factor is assumed in order to obtain the probability of failure.

# 3. Reference case study

The probabilistic study proposed in this paper was carried out with reference to a specific, thoroughly investigated 20 m-long segment of the river Secchia banks (northern Italy), which suddenly collapsed after a period of intense rainfall, in January 2014 (Figure 1). This section

provides a brief description of the detailed and rather varied geotechnical database collected after the bank failure in order to obtain information related to the collapse and used as reference dataset for the analyses contained herein.

As shown in Figure 2, the site investigation campaign was carried out along three main representative alignments: the first alignment was selected upstream from the collapsed river embankment section, approximately 900 m distant from the breach, the second was located in front of the collapsed area, on the opposite river embankment, whilst the third was placed next to the breach, only a few meters away on the downriver side. For each alignment, a borehole (BH) and a seismic piezocone test (SCPTU) were carried out from the crest of the river embankment and pushed to approximately 30 m in depth; two additional piezocone tests (CPTU) were carried out at the berm and close to the outer slope toe. The latter tests were stopped at different depths, from 14 to 26 m, depending on their position on the river embankment. A few dissipation tests were also carried out along each piezocone vertical, in order to monitor the pore water pressure decay with time and to evaluate the consolidation characteristics of fine sediments.

The laboratory experimental programme, carried out on a total of 27 undisturbed soil samples, included a significant number of tests for the determination of basic physical properties of soils, Atterberg limits, particle size distribution, in conjunction with a few oedometer tests, direct shear tests, drained (TXCD) and undrained (TXCU) triaxial tests to estimate the mechanical parameters of sediments. In addition, series of evaporation tests were performed for the estimation of the retention and hydraulic properties of the river embankment soil in partially-saturated conditions.

## 3.1 In situ testing interpretation

The subsoil beneath the collapsed river embankment stretch mainly consists of Pleistocene alluvial sediments resulting from depositional and erosional process of the Secchia and Panaro rivers, both draining a significant part of the Emilian Apennines into the major Italian watercourse Po.

Figure 3 shows the profiles of the corrected cone resistance $q_t$, sleeve friction $f_s$ and pore pressure $u$

196 obtained from the representative piezocone test SCPTU 7, located on the river embankment crest in
197 Section No. 3, the latter being depicted here according to its geometry after collapse. The
198 interpretation of piezocone data in terms of the well-known classification framework proposed by
199 Robertson [38], aimed at identifying the in situ Soil Behaviour Type (*SBT)*, and the actual soil
200 stratigraphy provided by the adjacent borehole BH-3 are also reported in the figure. Despite a few
201 discrepancies observed between CPTU-based classification results and the stratigraphy from
202 boreholes, presumably due to the combined effect of suction above phreatic surface, simplified
203 evaluation of effective stress state within the bank and partial drainage during cone penetration
204 testing [39], the comparative analysis of field data allows identifying three main soil units. As
205 shown in Figure 4 with respect to the cross-section No. 3, the stratigraphic arrangement includes:

206 • a 5 m thick, rather heterogeneous top layer of sands, silty sands and sandy silts (labelled as
207 *Unit R*), forming the artificial river embankment;
208 • a predominantly silty unit (*Unit B*), 5 to 12 m thick, referable to the flood plain environment
209 and corresponding to the upper part of the river embankment foundation subsoil;
210 • a clayey layer, detected at 12 to 30 m in depth from the bank crest, labelled as *Unit C*.

211 In this stratigraphic scheme, the groundwater table is located at approximately 6 m from the crest of
212 the reshaped bank, at 30 m above mean sea level, i.e. close to the transition surface between *Unit R*
213 and *Unit B,* as suggested by field data provided by the Casagrande-type piezometer installed into
214 borehole BH-3 as well as by interpretation of CPTU pore pressure profiles. Such phreatic surface
215 was found to be slightly sloping landwards, the hydraulic gradient $i$ being equal to 4%. Similar
216 stratigraphic arrangements and groundwater conditions were also identified from interpretation of
217 site investigations located along alignments No. 1 and No. 2, although a certain horizontal spatial
218 variability, in terms of both thickness and fine content of soil units *R* and *B* was observed. For this
219 reason, the geotechnical model discussed in this study is specifically pertinent to section No. 3 (i.e.
220 the closest alignment to the collapsed river embankment segment), whereas the geotechnical models
221 of the other sections will not be presented because out of scope.

222 Accordingly, the geotechnical characterization of the different soil units relied on CPTU and
223 SCPTU carried out in section No. 3, by applying semi-empirical correlations to field data. Results
224 from laboratory tests were used as reference in order to validate the estimates of the mechanical
225 parameters from in situ testing. The comparison between laboratory and field test results was
226 mainly restricted to sediments forming the river embankment, since most of the samples were
227 recovered in the upper 6 m. Furthermore, in view of the probabilistic analyses described in next
228 sections, attention was primarily focused on the evaluation of the effective shear strength of the soil
229 units. In particular, following previous successful experiences on natural silty mixtures referable to
230 a very similar depositional environment of the Po river basin [40], the drained shear strength of *Unit*
231 *R* and *Unit B*, expressed in terms of the effective friction angle at peak $\varphi'$, was determined using the
232 well-established correlation proposed by Kulhawy and Mayne [41]. As regards the fine-grained
233 *Unit C*, the estimates of $\varphi'$ were instead obtained from an effective stress limit plasticity solution
234 [42] whose effectiveness was proved on a large database of natural clays [43]. This approach is
235 based on the assumption that the effective cohesion intercept $c'$ is equal to 0, as reasonable in
236 normally consolidated clays like those of *Unit C*.
237 Figure 3e shows estimates of $\varphi'$ obtained from SCPTU7. The resulting profile exhibits an initial
238 decreasing trend in the upper portion of *Unit R*, referable to a sort of thin "crust" typically detected
239 by cone penetration or dilatometer tests in the topmost soil layers of the Po river basin
240 embankments (e.g. [40,44]) and likely due to overconsolidation for desiccation-wetting cycles
241 together with partial saturation effects. As a results, the values of $\varphi'$ computed in this shallow thin
242 lense were not considered as representative of *Unit R* and thus excluded from the statistical analysis
243 presented herein.
244 Table 1 provides a summary of the statistical parameters computed for the effective shear strength
245 of the different soil units, as obtained from the combined interpretation of SCPTU7, CPTU8 and
246 CPTU9. The skewness of $\varphi'$ was always set equal to zero, as a consequence of the virtually

symmetrical data distribution. It is worth observing that the range obtained for $\varphi'$ in *Unit R* (32°±1.9°) is fully consistent with the values (31.1°-34°) provided by triaxial tests, whereas in *Unit B* the effective friction angle from a few laboratory tests turned out to be close to the upper boundary identified by the statistical moments of Table 1. Unfortunately, laboratory test results in shearing were not available for *Unit C*, thus preventing any comparison between estimates of $\varphi'$. It is also interesting to notice that the values presented in Table 1 are consistent with those reported in the study of Phoon and Kulhawy [45], which was based on an extensive literature review.

Finally, it must be mentioned that the uncertainties on $\varphi'$ shown above do not include the so-called "transformation model" uncertainty, the attention being here primarily focused on the variability of the mechanical (and hydraulic) parameters as a consequence of the inherent heterogeneity of the investigated sediments. Nevertheless, it is worth emphasizing that, according to the recent study of Ching et al. [46], the CPT-$\varphi'$ transformation model [41] adopted in the present work for *Unit R* and *Unit B* was found to be nearly unbiased and with a broad application range.

| **Soil** | **Friction angle $\varphi'$ (°)** | | |
|---|---|---|---|
| **type** | mean value | standard deviation | skewness |
| *Unit_R* | 32.0 | 1.90 | 0 |
| *Unit_B* | 28.8 | 3.20 | 0 |
| *Unit_C* | 24.9 | 2.40 | 0 |

Table 1 – Statistical parameters (mean, standard deviation and skewness) of the friction angle **φ'**, for *Unit R*, *Unit B* and *Unit C*.

## 3.2 Unsaturated soil properties from evaporation tests

In order to characterize the soils forming the river embankment with respect to their hydraulic and retention response, series of evaporation tests were performed on nine undisturbed samples purposely collected near Section No. 3, at depths between 0.7 m and 1.7 m from the crest. Attention was obviously focused on sediments of the river embankment top layer *Unit R*, where unsaturated

conditions are likely to apply. All tests were performed according to the procedure proposed by Romano and Santini [47], which relies on a parameter optimization strategy for the determination of unsaturated soil properties using evaporation data. In this study, the well-known and widely-used hydraulic model proposed by van Genuchten [48] was adopted to fit the experimental data; thus, hysteresis in the typical water retention behaviour of unsaturated soils was disregarded for the prediction of the effective degree of saturation, $S_e$. Accordingly, this can be determined as follows:

$$S_e(h) = \frac{\theta - \theta_r}{\theta_0 - \theta_r} = \left[\frac{1}{1+(\alpha_{VG} \cdot s)^{n_{VG}}}\right]^{m_{VG}} \quad (11)$$

where $\theta$, $\theta_0$ and $\theta_r$ are the volumetric soil water content at the current stage, at saturation and in residual conditions respectively, $s$ is the soil suction, given by the difference between the pore air pressure, $u_a$, and the pore water pressure, $u_w$, whilst $\alpha_{VG}$ and $n_{VG}$ are model parameters, mainly influencing the inflection and the shape of the retention curve respectively. Some authors [49] also refer to $\alpha_{VG}$ as the inverse of suction value at which the soil starts to desaturate. It is useful to remind that $n_{VG}$ and $m_{VG}$ are usually considered as inter-dependent parameters, defined as:

$$m_{VG} = 1 - \frac{1}{n_{VG}} \quad (12)$$

In accordance with the Mualem's [50] model coupled with the parametrisation procedure suggested by van Genuchten [48], the variation of soil permeability with suction was derived from the Soil Water Retention Curve (SWRC), which describes the relationship between volumetric water content and matric suction. Hence, the following equation was used:

$$k_r = {S_e}^{0.5}\left[1 - \left(1 - {S_e}^{1/m}\right)^m\right]^2 \quad (13)$$

The above equation, typically referred to as Hydraulic Conductivity Function, defines the relationship between the effective degree of saturation, $S_e$, and the relative permeability, $k_r$. The hydraulic permeability of the soil is then obtained as the product of the saturated permeability, $k_0$, and the relative permeability, $k_r$.

Figure 5 shows the SWRCs obtained by fitting the available laboratory data using eq.(11). The plot provides the effective degree of saturation $S_e$ as a function of suction $s$. Although all the samples

were taken from the same soil unit, a significant degree of heterogeneity is observed on the hydraulic behaviour of the soil in partially saturated conditions.

Based on such experimental results, a statistical interpretation of the hydraulic parameters of *Unit R*, expressed in terms of mean values, standard deviation, skewness and correlation structure, was carried out. It is worth observing that the amount of available laboratory test results can be considered as statistically significant for the proposed study, also considering that each evaporation test involved three independent measurements and that, at the same time, such dataset is significantly larger than those typically available in engineering practice. The computed mean values of the unsaturated hydraulic parameters of *Unit R*, together with standard deviation and skewness are listed in Table 2, whilst the relevant correlation matrix is provided in Table 3. The parameter $m_{VG}$ was obviously excluded from the list of hydraulic input variables, being dependent on $n_{VG}$.

**Hydraulic parameters of *Unit R***

| | mean value | standard deviation | skewness |
|---|---|---|---|
| $\theta_r$ [m$^3$/m$^3$] | 0.079 | 0.078 | 0.542 |
| $\theta_{sat}$ [m$^3$/m$^3$] | 0.395 | 0.041 | 0.026 |
| $\alpha_{VG}$ [kPa$^{-1}$] | 0.164 | 0.064 | -0.824 |
| $n_{VG}$ [-] | 1.328 | 0.154 | 0.016 |
| log ($k_0$) [log(m/s)] | -5.805 | 0.776 | -0.632 |

Table 2 – Statistical moments (mean, standard deviation and skewness) of the unsaturated hydraulic parameters of soil *Unit R*.

| | $\boldsymbol{\theta_r}$ m$^3$/m$^3$ | $\boldsymbol{\theta_{sat}}$ m$^3$/m$^3$ | $\boldsymbol{\alpha_{VG}}$ kPa$^{-1}$ | $\boldsymbol{n_{VG}}$ - | $\boldsymbol{\log(k_0)}$ log(m/s) |
|---|---|---|---|---|---|
| $\boldsymbol{\theta_r}$ | 1 | 0.0 | 0.0 | 0.37 | -0.51 |
| $\boldsymbol{\theta_{sat}}$ | - | 1 | 0.34 | 0.69 | 0.63 |
| $\boldsymbol{\alpha_{VG}}$ | - | - | 1 | –0.09 | 0.68 |
| $\boldsymbol{n_{VG}}$ | - | - | - | 1 | 0.23 |
| $\boldsymbol{\log(k_0)}$ | - | - | - | - | 1 |

Table 3 – Correlation matrix of the unsaturated hydraulic properties of soil *Unit R*.

It is worth mentioning that the statistical moments shown in Table 2 fall in the ranges typically reported in the literature. Indeed, according to a number of studies (e.g. [20,51-52]), based on either direct or indirect methods for the assessment of hydraulic parameters, typical ranges of the coefficient of variation ($CoV_{(X)} = \sigma_X/\mu_X$) of the Van Genuchten – Mualem model parameters are: $CoV_{(\theta_r)}$= 10-110%, $CoV_{(\theta_{sat})}$ = 5-25%, $CoV_{(\alpha_{VG})}$ = 20-100%, $CoV_{(n_{VG})}$ = 3-20%, $CoV_{(k_0)}$ = 100-300%. Besides, the mean values of Table 2 turn out to be fully consistent with those reported by Santoso et al. [53]. Regarding *Unit B* and *Unit C*, only the permeability at saturation, $k_0$, was taken into account, since both units are permanently below the phreatic line. Mean values of the permeability, as obtained from the application of empirical correlations to piezocone data [54], turn out to be $1.88 \cdot 10^{-6}$ m/s and $1.30 \cdot 10^{-9}$ m/s for *Unit B* and *Unit C,* respectively. It must be emphasized that the permeability of both units was considered as a deterministic parameter in the probabilistic analyses proposed herein.

# 4. Development of the seepage model for the stability analyses in transient conditions

The seepage and stability analyses were carried out with reference to a 2D river embankment model based on the geometry, stratigraphic conditions, geotechnical and hydrological data of section No. 3 of the river Secchia (Figure 4), as it used to be prior to failure, i.e. 7 m high, with the outer and inner slope angles equal to 30° and 33° respectively. In order to properly assess the stability of an existing river embankment with respect to a specific flooding event, it is necessary to undertake transient seepage analyses, accounting for both river level fluctuations and rainfall infiltration, starting from realistic initial conditions. Accordingly, the soil forming the river embankment, namely soil Unit *R* in this study, must be assumed as partially saturated, with relevant implications on both the seepage process and soil shear strength that will be discussed later. In particular, in the absence of specific measurements for the studied river embankment segment, a suitable initial suction distribution into the bank, which might be considered as typical during a period of

365 significant rainfall events, was firstly sought. Following previous experiences of other Authors (e.g.
366 [1,55-58]), the distribution eventually adopted assumes that suction is maximum in the river
367 embankment core and approximately equal to zero at the free surface.
368 As a result, taking the water table at 30 m above the means sea level (m.s.l.), close to the transition
369 surface between *Unit R* and *Unit B* (see Fig. 4), suction was assumed to linearly increase up to 39
370 kPa in correspondence of the centre of the bank, at 4 meters above the phreatic line, and then to
371 decrease to zero close to the bank crest.
372 Flow through an earthen structure highly depends on the relative permeability of the fill material,
373 which in turn depends on its degree of saturation. The transient unsaturated-saturated flow was
374 modelled using the 2D Finite Element code SEEP/W [59], assuming the effective degree of
375 saturation and the relevant hydraulic permeability derived from the application of the van
376 Genuchten-Mualem model [48], as discussed in §3.2. The FE numerical solution is based on the
377 Generalized Darcy Law for transient seepage conditions, given by:
378 (14) $$\boldsymbol{q} = \frac{\partial \theta}{\partial t} - k_r k_0 \nabla \left( \frac{u_w}{\gamma_w} + z \right)$$
379 where $z$ is the vertical elevation and $\boldsymbol{q}$ is the boundary flux per unit area. When the water storage in
380 the model does not vary with time, steady-state conditions apply, basically corresponding to
381 significantly high persistency of the hydrometric peak.
382 Positive and negative pore water pressure distributions obtained at the end of the seepage analysis
383 were then imported into the code SLOPE/W [60] and assumed as input data for the riverbank
384 stability calculations, using limit equilibrium methods. Among the different available approaches,
385 the Morgenstern and Price [61] method was eventually selected to perform the stability analyses in
386 transient flow conditions.
387 Slip surfaces were generated randomly, according to suitable pre-defined geometrical constraints,
388 consisting in the ranges for the entry zone and the exit zone of the sliding mechanism on the ground
389 surface, together with the so-called “minimum depth” (corresponding to the minimum height of

LEM slices). In this way, a significant collapse mechanism could be identified, while excluding potential local shallow slip surfaces (see Fig. 6). The minimum slip surface depth was assumed to be 1.5 m and 3.8 m for the inner and outer instability mechanisms, respectively. Furthermore, the potential slip surfaces were all circular, as actually observed in the collapse occurred in January 2014.

Regarding soil shear strength, the limit equilibrium analyses performed in this study made use of the Vanapalli et al. [62] failure criterion, which is implemented in SLOPE/W. As many other strength criteria for unsaturated soils, this approach derives from the linear shear strength equation originally proposed by Fredlund et al. [63], extending such formulation to account for the impact of non-linearity of the soil water retention curve on the resulting shear strength relationship. As a result, the shear strength of an unsaturated soil is assumed to vary with the degree of saturation ($S_e$) and the matric suction ($u_a - u_w$), according to the following expression:

$$\tau = c' + (\sigma_n - u_a)tan\varphi' + (u_a - u_w)S_e tan\varphi' \quad (15)$$

with $\sigma_n$ = the total normal stress, $c'$ = effective cohesion, $\varphi'$ = effective stress friction angle.

The first part of the equation describes the saturated shear strength, which is a function only of the normal stress since the shear strength parameters $c'$ and $\varphi'$ are assumed as constant for a saturated soil. The second part [i.e., $(u_a - u_w)\cdot S_e \cdot tan\varphi'$] provides the shear strength contribution due to suction, which can be predicted using the soil water retention curve [64]. In particular, the formulation described by eq.(15) fulfils a number of well-known experimental evidences reported by various Authors (e.g. [62,65]): when the soil begins to desaturate, the unsaturated soil strength contribution varies according to a non-linear function of suction, as long as the matric suction remains above the air entry value (AEV), this latter corresponding to the point at which air enters the largest pores of the soil [50]. By contrast, when suction is below AEV, the unsaturated shear strength is equal to $(u_a - u_w)\cdot \tan\varphi'$. In saturated conditions, when the pore-air pressure, $u_a$, is equal to the pore-water pressure, $u_w$, eq. (15) turns into the classical Mohr – Coulomb failure criterion.

With respect to the shear strength values adopted in the analyses, a few points must be emphasized. First of all, it is worth remarking that the use of data only from the evaporation tests prevented from dealing with soil hysteresis in the water retention behaviour. As a matter of fact, the seepage process to be modelled in this study is not truly referable to wetting paths, but rather to scanning paths, which in turn would require specific laboratory tests for characterization. On the other hand, a few preliminary analyses based on the parameters estimated for the wetting branch, according to suggestions of Likos et al. [52], showed that the use of data from a main drying curve generally does not provide results on the unsafe side in terms of reliability assessment, which is indeed the main focus of this study. This outcome is due to a combination of different governing factors that result in opposite effects on the numerical assessment of the riverbank stability and the prevalence of one effect on the others should be analysed in each specific case. Indeed, although the assumption of non-hysteretic hydraulic behaviour might tend to overestimate the suction values for an assigned effective degree of saturation, the relative permeability would be then underestimated by the van Genuchten model, with evident consequences on the flow regime and leading, at the end of high water events, to a minor impact on the phreatic line, particularly when initial conditions are defined in terms of suction.

# 5. Probabilistic stability analysis

The probabilistic analysis of the riverbank stability was organized into two main stages, referred to as “First-level probabilistic analysis” and “Second-level probabilistic analysis” respectively. The first includes a few preliminary analyses based on the assumption that the soil friction angle φ' is the only random variable. Both steady-state seepage conditions, typically suggested by guidelines, and transient seepage in partially saturated soils, were modelled. Indeed, although the steady-state seepage turns out to be the most critical situation for the stability of a river embankment, only a transient seepage approach, accounting for fluctuations of the river water level and rainfall

infiltration, can realistically identify the actual margins of safety of the structure during a specific flooding event. Obviously, the variability of the friction angle has no effects on the finite element seepage analysis, thus only affecting slope stability results.

By contrast, in the "Second-level probabilistic analysis", the riverbank reliability analysis was carried out solely under transient seepage conditions, accounting for uncertainties in both the effective friction angle and the unsaturated soil hydraulic parameters. In this way, the different impact produced by different sources of uncertainties in soil parameters may be identified.

At this point, it must be observed that a comprehensive stochastic analysis of the seepage through the river embankment should also consider the aleatory uncertainty associated with the initial pore water pressure distribution [66], which in turn depends on the river water level fluctuations. In this study, however, such aspect was disregarded, being the attention basically focused on the variability of geotechnical parameters and its effects on the riverbank reliability.

## 5.1 First-level probabilistic analysis

### *5.1.1 Steady state conditions*

The steady state seepage analysis was performed assuming the river level at the maximum hydrometric height recorded during the January 2014 flooding event, i.e. at 35.9 m above mean sea level [21], whilst the water table on landward side was located at the ground level. Constant values of the hydraulic conductivities were adopted for the different soil units, namely equal to the saturated permeability $k_0$ reported in Table 2 for *Unit R* and to the values of $k_0$ mentioned in § 3.2 for *Unit B* and *Unit C*. Figure 7 shows the computed pore water pressure (PWP) and the corresponding pressure head distributions, used in turn as input for the limit equilibrium analyses. The latter are based on the assumption that the soil shear strength obeys the effective stress Mohr-Coulomb failure criterion and that the friction angle of the river embankment soil unit (*Unit R*) follows a normal distribution, described by the statistical moments reported in Table 1 (mean shear

strength = 32.0°, standard deviation = 1.9°). In these analyses, the contribution to shear strength due to suction is disregarded. The shear strength parameters of the underlying soil units, i.e. *Unit B* and *Unit C,* were considered as deterministic variables, the main goal being to investigate the effect of soil strength variability only within the river embankment. In this case, the model uncertainty is described by just one random variable and therefore the application of the *Point Estimate Method* requires only two combinations. For each point estimate combination, the most critical slip surface, in terms of safety factor, was randomly searched.

As mentioned in §2, these preliminary analyses were performed using both PEM and MCM, in order to assess the accuracy of the probability of failure provided by the *Point Estimate Method* compared to results of the robust *Monte Carlo* approach, the latter requiring a relatively moderate computational effort when uncertainty in soil parameters is limited to a single random variable. Values of the safety factor and probability of failure obtained from the probabilistic analyses are summarized in Table 4. A substantial agreement between the MCM and PEM results can be observed in this case, thus providing support for the application of only the *Point Estimate Method* to the whole stability problem discussed in this paper. Agreement between the two probabilistic methods was also documented by Vannucchi [67] with respect to other geotechnical applications.

Probabilistic Analysis Results – Steady state seepage conditions – PEM and MCM

| Safety Factor | Outer slope | | Inner slope | |
|---|---|---|---|---|
| | PEM | MCM | PEM | MCM |
| Mean ($\mu_{SF}$) | 1.013 | 1.013 | 1.405 | 1.405 |
| Standard deviation ($\sigma_{SF}$) | 0.046 | 0.047 | 0.106 | 0.107 |
| Reliability index ( $\beta_{SF}$) | 0.283 | 0.274 | 3.821 | 3.791 |
| Probability of failure (%) | 38.9 | 39.9 | $6.7 \cdot 10^{-3}$ | $7.3 \cdot 10^{-3}$ |

Table 4 – Probabilistic results of limit equilibrium analyses in steady state condition, for outer and inner slopes, with deterministic soil bank hydraulic parameters.

485 It is worth observing that the stability analyses in steady seepage conditions, though not
486 representative for the specific flooding event, provide a sort of reference benchmark and useful
487 information with regard to the existing margin of safety of the river embankment. Indeed, according
488 to the computed values of the reliability index $\beta_{SF}$, which turn out to be very low, the stability of the
489 outer slope in case of persistent high river water levels appears critical. By contrast, a high
490 reliability index value (thus implying a low probability of failure) was obtained for the most critical
491 surface of the inner slope.
492
493 ### *5.1.2 Transient seepage conditions*
494 In transient seepage analyses, the river water level fluctuation was modelled as time-dependent
495 boundary condition on the riverside FE mesh nodes, expressed in term of total hydraulic head.
496 Rainfall infiltration was simulated as water flux through the boundary surface, based on the
497 hydrometric values and precipitation data recorded in close proximity to the investigated breached
498 area, from 25 December 2013 to the flooding event date (19 January 2014). The daily river levels
499 and rainfall recorded by the competent Regional Authority are plotted in Figure 8, together with the
500 approximated profile of the total hydraulic head variation versus time, applied at the riverside
501 boundary of the numerical model. Figure 9 shows the computed pore water pressure distributions at
502 the initial and final stage of transient seepage analysis. As regards the unsaturated hydraulic
503 parameters of *Unit R*, here treated as deterministic variables, the mean values of Table 2 were
504 adopted.
505 The subsequent probabilistic limit equilibrium analysis, based on the PEM approach, resulted in
506 very high values of the reliability index $\beta_{SF}$ (i.e. very low probabilities of failure), especially for the
507 inner slope (Table 5). Since the probability of failure provided by PEM may suffer from a lack of
508 accuracy at very small probability levels, in this study a threshold value equal to $10^{-3}$% was
509 assumed as reference for the minimum value of $P_f$, hence the reason for $P_f$ expressed as $<10^{-3}$% in

510 Table 5. On the other hand, probabilities of failure lower than $10^{-3}$% does not seem to provide
511 additional information with respect to the riverbank stability conditions.
512

Probabilistic Analysis Results – Transient seepage conditions

| Safety Factor | Outer slope | Inner slope |
|---|---|---|
| Mean ($\mu_{SF}$) | 1.346 | 2.077 |
| Standard deviation ($\sigma_{SF}$) | 0.063 | 0.156 |
| Reliability index ( $\beta_{SF}$) | 5.492 | 6.904 |
| Probability of failure ($P_f$, %) | $< 10^{-3}$ | $< 10^{-3}$ |

513 Table 5 – Probabilistic results of M-P limit equilibrium analyses in transient seepage condition, for
514 outer and inner slopes, with deterministic soil bank hydraulic parameters.
515

## 516 5.2 Second-level probabilistic analysis

517 The second-level probabilistic analysis was performed in order to investigate the effect of multiple
518 sources of uncertainties in soil parameters (i.e. both shear strength and unsaturated hydraulic
519 properties) on the assessment of riverbank stability, expressed in terms of the degree of uncertainty
520 associated with the safety factor.
521 For this purpose, three different sets of probabilistic analyses were devised, according to the
522 different assumptions adopted in the cases specified below:
523 *Case 1*: friction angle ($\varphi'$) of *Unit R* assumed as random variable and hydraulic parameters ($\vartheta_r$, $\vartheta_0$,
524 $\alpha_{VG}$, $n_{VG}$, $k_0$) as deterministic variables, equal to their mean values.
525 *Case 2*: shear strength angle ($\varphi'$) and hydraulic parameters ($\vartheta_r$, $\vartheta_0$, $\alpha_{VG}$, $n_{VG}$, $k_0$) of *Unit R* assumed
526 as non-correlated random variables.
527 *Case 3*: shear strength angle ($\varphi'$) and hydraulic parameters ($\vartheta_r$, $\vartheta_0$, $\alpha_{VG}$, $n_{VG}$, $k_0$) of *Unit R* assumed
528 as correlated random variables.
529 As a matter of fact, *Case 1* corresponds to the first-level probabilistic analysis in transient seepage
530 condition commented in § 5.1.2.

531 The remaining two cases were analysed following the methodological approach already described,
532 i.e. transient seepage analyses were carried out using appropriate hydraulic soil parameters and
533 then, based on the computed pore water pressure distributions, for each point estimate combination
534 the most critical slip surface was randomly searched. Hence, such analyses are not based on a
535 deterministic choice of a predefined critical failure surface, which therefore may vary as different
536 point estimate combinations are adopted. In both *Case 2* and *Case 3*, probabilistic analyses
537 considered a total of 6 random variables: the friction angle $\varphi'$ and 5 hydraulic parameters ($\theta_r$, $\theta_{sat}$,
538 $\alpha_{VG}$, $n_{VG}$, $k_0$) of *Unit R*. In this way, the application of PEM resulted in 64 combinations of point
539 estimate locations. Histograms of each random variable, together with the indication of the point
540 estimate locations ($X_+$ and $X_-$) and the associated weights ($P_+$ and $P_-$), are shown in Figure 10.
541 The method consists in calculating the safety factor *SF* for each set of parameters in a deterministic
542 way. According to the procedure described in § 2.1, results were then suitably processed in order to
543 obtain the mean $\mu_{SF}$ and the standard deviation $\sigma_{SF}$ of safety factor *SF*, assumed as a normally
544 distributed random variable.
545

546 # 6. Discussion of results

547 Results of the probabilistic analyses for the three cases investigated in the second-level probabilistic
548 analysis are summarized in Figures 11 and 12, plotted in terms of probability density function
549 (PDF) of the safety factor, cumulative density function (CDF) and probability of failure ($P_f$)
550 associated with the safety factor, for both the outer and the inner riverbank slopes. It is worth
551 mentioning here that the probability of failure can be easily determined from the cumulative density
552 function for a safety factor equal to 1 ($CDF_{SF=1}$), since $P_f$ (%) = 100 x $CDF_{SF=1}$.
553 Figure 11 clearly shows that the mean value of the safety factor is approximately equal to 1.3 for
554 the outer slope and close to 2.0 for the inner slope, with minor differences among the three cases
555 mentioned above. Hence, the riverside zone appears to be significantly more stable than the

556 landward zone. In general, it is immediate to observe that for this case study standard safety factors
557 are sufficiently high; in fact, with regards to the most probable causes of the sudden collapse
558 occurred in January 2014, other possible local structural weaknesses – like the extensive presence
559 of animal burrows – were eventually advocated having triggered the catastrophic event [21].
560 However, this probabilistic study allows identifying very significant differences in the evaluation of
561 the riverbank reliability, as a consequence of the different assumptions adopted in the three series of
562 numerical analyses, which deserve particular attention in the light of common risk assessment
563 procedures. In *Case 2* and *Case 3*, both accounting for the variability of hydraulic parameters in
564 addition to shear strength, the uncertainty degree in the estimate of the safety factor increases
565 considerably, with associated rather low values of the reliability index $\beta$, always lower than 3.5.
566 Accordingly, the probability of failure turns out to be non-negligible, namely higher that $10^{-2}$% for
567 both the inner and outer slope, whilst extremely low values of $P_f$ (< $10^{-3}$ %) were obtained when the
568 only source of uncertainty was assumed to lie in shear strength (*Case 1*).
569 In particular, the probability density functions plotted in Figure 11 provide clear evidence of an
570 increase in the standard deviation of the safety factor when the stability analyses are carried out
571 under stochastic unsaturated transient seepage conditions. The effect may be appreciated in both
572 riverbank slopes, although it is undoubtedly more noticeable for the riverside stability analyses,
573 being the shape of the probability distributions associated with *Case 2* and *Case 3* significantly
574 wider than the "thin" shape of *Case 1*.
575 Besides, the probability of failure provided by the numerical analyses of *Case* 3, reflecting the
576 uncertainties of the unsaturated hydraulic parameters as well as their correlation structure, is one
577 order of magnitude smaller than that obtained in *Case* 2, the latter being based on the assumption of
578 no correlation between the parameters. Such outcome is consistent with results reported by Zhang et
579 al. [68-69] with respect to slope stability problems. Indeed, additional information on the input
580 parameters result in a better knowledge of them, thus leading to a reduction of the degree of
581 uncertainty. This point was extensively discussed also by Phoon et al. [20], who observed that

582 correlations between unsaturated hydraulic parameters should be investigated as a preliminary step
583 in any probabilistic study instead of assuming a priori their independence for expediency.
584 Furthermore, Figure 13 shows results of a sensitivity analysis on the input parameters, i.e. shear
585 strength and hydraulic parameters, aimed at investigating their relative importance on the river
586 embankment response. Such relative contribution was quantified in terms of the variance of the
587 safety factor, $\sigma_{SF}^2$, defined according to eq.(8). In particular, the contribution of the hydraulic
588 parameters to $\sigma_{SF}^2$ was simply evaluated as the difference between the safety factor variance
589 computed in *Case 2* ($\sigma_{SF,c2}^2$) or, alternatively, in *Case 3* ($\sigma_{SF,c3}^2$) and the safety factor variance
590 associated with *Case 1* ($\sigma_{SF,c1}^2$), the latter being based on the uncertainty in shear strength (φ') only.
591 Accordingly, for *Case 2* and *Case 3*, the per cent relative contribution of the effective friction angle
592 ($\sigma_{\%,\varphi'}^2$) and the hydraulic parameters ($\sigma_{\%,hp}^2$) to the safety factor variance can be evaluated as
593 follows:

594 (16a) $\sigma_{\%,\varphi'}^2 = 100 \cdot \sigma_{SF,c1}^2/\sigma_{SF,c2}^2$ *Case 2*

595 or

596 (16b) $\sigma_{\%,\varphi'}^2 = 100 \cdot \sigma_{SF,c1}^2/\sigma_{SF,c3}^2$ *Case 3*

597 (17a) $\sigma_{\%,hp}^2 = 100 \cdot \left(\sigma_{SF,c2}^2 - \sigma_{SF,c1}^2\right)/\sigma_{SF,c2}^2$ *Case 2*

598 or

599 (17b) $\sigma_{\%,hp}^2 = 100 \cdot \left(\sigma_{SF,c3}^2 - \sigma_{SF,c1}^2\right)/\sigma_{SF,c3}^2$ *Case 3*

600 According to results plotted in Figure 13, the unsaturated hydraulic parameters appear to have the
601 largest influence on the uncertainty of the safety factor, with percentages of contribution in the
602 ranges 72-84% and 79-83% for the outer slope and inner slope respectively.
603 A final parametric study was undertaken in order to gain a better insight into the effect of the
604 coefficient of variation of the only friction angle φ', $CoV_{(\varphi')}$, on the probability of failure, with
605 respect to both riverbank slopes. For this purpose, three different values of $CoV_{(\varphi')}$, selected within

606 the typical interval (i.e. 5-15%) quoted for this statistical parameter by various authors (e.g.
607 [3,45,70,71]), were investigated, while assuming the unsaturated hydraulic properties either as
608 deterministic or correlated random variables. Results of these series of analyses, expressed in terms
609 of probability of failure versus $CoV_{(\varphi')}$, are plotted in Figure 14. For $CoV_{(\varphi')} = 6\%$, corresponding to
610 the value computed from the available experimental estimates, the values of $P_f$ coincide with those
611 previously calculated in *Case 1* (i.e. deterministic transient seepage) and *Case 3* (i.e. stochastic
612 transient seepage based on correlated hydraulic random variables).
613 As the coefficient of variation of the shear strength increases from 6% to 15%, the impact of $\varphi'$ on
614 the variance of the safety factor was found to consistently increase, causing in turn a decrease in the
615 relative importance of the hydraulic parameters on the output. However, Figure 14 clearly shows
616 that the difference between the probability of failure obtained under the opposite hypotheses of
617 stochastic and deterministic transient seepage remains significant as long as $CoV_{(\varphi')}$ does not exceed
618 10% for the outer riverbank slope and 15% for the inner slope.
619 This outcome demonstrates that for usual values of uncertainty degree of the effective friction
620 angle, the variability of the unsaturated soil hydraulic parameters plays a crucial role in the
621 assessment of the probability of failure of the riverbank slopes. Hence, neglecting the intrinsic
622 variability of such parameters, even in soils assumed as relatively homogenous from a geotechnical
623 point of view, may lead to estimates of the probability of failure which are not consistent with the
624 real risk and typically non conservative. Further investigations and additional datasets from specific
625 case studies are obviously required in order to confirm the above results and draw more
626 comprehensive conclusions.
627

628 # 7. Conclusions

629 This paper has presented a probabilistic study aimed at exploring the role of partial saturation of
630 soils and of intrinsic variability of the relevant hydraulic parameters, beside shear strength, on the

631 stability of existing river embankments. The issue has been discussed with reference to actual data
632 of a specific 20m-long stretch of the river Secchia banks (northern Italy), which was extensively
633 investigated following its catastrophic sudden collapse occurred in January 2014, after a period of
634 intense rainfall. The large and varied geotechnical database related to this case study has enabled
635 the development of a detailed geotechnical model of the breached segment, inclusive of the
636 mechanical and hydraulic behaviour of the sediments forming the unsaturated river embankment,
637 thus allowing sound probabilistic analyses supported by experimental results.
638 Uncertainties on geotechnical data are typically disregarded in standard practice and only a very
639 limited number of research contributions have considered the effect of the variability of hydraulic
640 soil properties on riverbank stability. Furthermore, according to recommendations of current
641 geotechnical codes and standards, the assessment of riverbank stability is generally based on the
642 over-simplified assumption of steady state seepage in equilibrium with the highest possible river
643 level.
644 In this study, three key features have been taken into consideration: 1) the time-dependent hydraulic
645 boundary conditions due to water level fluctuations in the river, thus requiring a transient seepage
646 analysis; 2) the unsaturated initial state of the river embankment; 3) the uncertainty in the
647 geotechnical parameters, including those describing the unsaturated behaviour of sediments.
648 The probabilistic analyses have been carried out using the Point Estimate Method, a widely
649 recognized procedure for slope reliability analyses, which appears to offer significant advantages in
650 terms of efficiency over the more robust Monte Carlo method where the assessment of the
651 probability of failure can be computationally intensive.
652 The reason for adopting this simplified uncertainty propagation method is twofold. Infact, apart
653 from its efficiency and rather straightforward implementation procedure, which make the approach
654 attractive for use also in routine risk analyses, the idea behind the study is basically to explore the
655 relative weight of a number of random variables on the stability assessment of a river embankment,
656 expressed in terms of probability of failure.

Although the actual safety factors of both inner and outer slopes of the Secchia river embankment are generally far from unity, thus suggesting that the January 2014 failure should be most likely seen as due to lack of local integrity for animal burrows, the results presented in this paper have proved that the probability of failure is strongly influenced by the suction distribution, which in turn depends on the hydraulic parameters adopted in the analyses. When uncertainty in unsaturated hydraulic parameters is taken into account, the probability of failure turns out to be significantly higher than that obtained on the assumption that shear strength is the only random variable, the difference being in this case of various orders of magnitude. This study has also shown that for the usual uncertainty degree of shear strength, the variability of the unsaturated soil hydraulic parameters has a major impact on the resulting probability of failure, for both riverbank slopes. Hence, not only the unsaturated transient seepage conditions are of outmost importance in the assessment of riverbank stability, but also underestimating the effect of the intrinsic variability of hydraulic parameters, even in soils assumed as relatively homogenous, may lead to probabilities of failure which are not consistent with the actual risk and potentially non-conservative. The latter aspect, which is typically neglected in routine risk assessment procedures either for lack of relevant experimental data or lack of awareness of the potential consequences, should be taken in careful consideration instead.

Further investigations and additional datasets from specific case studies would be required in order to confirm the results discussed in this study and draw more comprehensive conclusions. It is finally worth observing that, in spite of a certain roughness, the Point Estimate Method has proved to clearly capture the effect of the intrinsic variability of the unsaturated soil hydraulic properties on the reliability analysis of the river embankment.

# References

[1] Rinaldi M, Casagli N, Dapporto S, Gargini A. Monitoring and modelling of pore water

682 pressure changes and riverbank stability during flow events. Earth Surf Process Landforms
683 2004;29(2):237–54. doi:10.1002/esp.1042.
684 [2] Liang C, Jaksa MB, Ostendorf B, Kuo YL. Influence of river level fluctuations and climate
685 on riverbank stability. Comput Geotech 2015;63:83–98. doi:10.1016/j.compgeo.2014.08.012.
686 [3] Baecher GB, Christian JT. Reliability and Statistics in Geotechnical Engineering. 2003.
687 [4] Ching J, Phoon KK. Establishment of generic transformations for geotechnical design
688 parameters. Struct Saf 2012;35:52–62. doi:10.1016/j.strusafe.2011.12.003.
689 [5] Low BK. FORM, SORM, and spatial modeling in geotechnical engineering. Struct Saf
690 2014;49:56–64. doi:10.1016/j.strusafe.2013.08.008.
691 [6] Aguilar-López JP, Warmink JJ, Schielen RMJ, Hulscher SJMH. Soil stochastic parameter
692 correlation impact in the piping erosion failure estimation of riverine flood defences. Struct
693 Saf 2016;60:117–29. doi:10.1016/j.strusafe.2016.01.004.
694 [7] Zhao T, Montoya-Noguera S, Phoon K-K, Wang Y. Interpolating spatially varying soil
695 property values from sparse data for facilitating characteristic value selection. Can Geotech J
696 2018;55:171–181. doi:10.1139/cgj-2017-0219.
697 [8] Zhang L, Li J, Li X, Zhang J, Zhu H. Rainfall-Induced Soil Slope Failure: Stability Analysis
698 and Probabilistic Assessment. CRC Press, Taylor & Francis Ltd, London, United Kingdom,
699 2019.
700 [9] Christian BJT, Ladd CC, Baecher GB. Reliability Applied to Slope Stability Analysis. J
701 Geotech Eng 1994;120(12):2180–207.
702 [10] Husein Malkawi AI, Hassan WF, Abdulla FA. Uncertainty and reliability analysis applied to
703 slope stability. Struct Saf 2000;22:161–87. doi:10.1016/S0167-4730(00)00006-0.
704 [11] Ranalli M, Medina-Cetina Z, Gottardi G, Nadim F. Probabilistic calibration of a dynamic
705 model for predicting rainfall-controlled landslides. Journal of Geotechnical and
706 Geoenvironmental Engineering 2014;140(4):4013039.
707 [12] Jiang SH, Huang JS. Efficient slope reliability analysis at low-probability levels in spatially

708 variable soils. Comput Geotech 2016;75:18–27. doi:10.1016/j.compgeo.2016.01.016.
709 [13] Zhang J, Huang HW, Zhang LM, Zhu HH, Shi B. Probabilistic prediction of rainfall-induced
710 slope failure using a mechanics-based model. Engineering Geology 2014;168:129-40.
711 doi:10.1016/j.enggeo.2013.11.005
712 [14] Santoso A, Phoon KK, Quek ST. Effects of soil spatial variability on rainfall-induced
713 landslides. Computers and Structures 2011;89(11–12):893-900.
714 doi:10.1016/j.compstruc.2011.02.016
715 [15] Tung YK, Chan GCC. Stochastic analysis of slope stability considering uncertainties of soil-
716 water retention characteristics. In: Proceedings 9th Int. Conf. on Applications of Statistics and
717 Probability in Civil Engineering; 2003. p. 1409–14.
718 [16] Zhang LL, Zhang LM, Tang WH. Rainfall-induced slope failure considering variability of
719 soil properties. Géotechnique 2005;55(2):183–88.
720 [17] Liu K, Vardon PJ, Hicks MA, Arnold P. Combined effect of hysteresis and heterogeneity on
721 the stability of an embankment under transient seepage. Eng Geol 2017;219:140–50.
722 [18] Cho SE. Probabilistic analysis of seepage that considers the spatial variability of permeability
723 for an embankment on soil foundation. Eng Geol 2012;133–134:30–9.
724 [19] Le TMH, Gallipoli D, Sanchez M, Wheeler SJ. Stochastic analysis of unsaturated seepage
725 through randomly heterogeneous earth embankments. Int J Numer Anal Methods Geomech
726 2012;36:1056–76. doi:10.1002/nag.1047.
727 [20] Phoon K-K, Santoso A, Quek S-T. Probabilistic Analysis of Soil-Water Characteristic
728 Curves. J Geotech Geoenvironmental Eng 2010;136:445–55.
729 [21] D'Alpaos L, Brath A, Fioravante V. Relazione tecnico-scientifica sulle cause del collasso
730 dell ' argine del fiume Secchia avvenuto il giorno 19 gennaio 2014 presso la frazione San
731 Matteo. Http://AmbienteRegioneEmilia-RomagnaIt/Geologia/Notizie/Notizie-2014/Fiume-
732 Secchia 2014.
733 [22] Wolff TF. Probabilistic slope stability in theory and practice. In: C.D. Shackelford PPN and

734 MJSR, editor. Uncertain. Geol. Environ., University of Wisconsin–Madison Press; 1996, p.
735 419–33.
736 [23] Duncan JM. Factors of Safety and Reliability in Geotechnical Engineering. J Geotech
737 Geoenvironmental Eng 2000;126:307–16. doi:10.1061/(ASCE)1090-0241(2000)126:4(307).
738 [24] Vannucchi G, Gottardi G, Madiai C, Marchi M, Tonni L. Analisi della probabilità di collasso
739 arginale dei grandi fiumi. Atti del XXV Convegno Naz. di Geotec., Baveno, Italy: 2014, p.
740 303–19.
741 [25] Ahmed A, Soubra AH. Probabilistic analysis at the serviceability limit state of two
742 neighboring strip footings resting on a spatially random soil. Struct Saf 2014;49:2–9.
743 [26] Li D, ChenYF, Lu WB, Zhou CB. Stochastic response surface method for reliability analysis
744 of rock slopes involving correlated non-normal variables. Computers and Geotecnics
745 2011;38(1):58-68.
746 [27] Au SK, Ching J, Beck JL. Application of subset simulation methods to reliability benchmark
747 problems. Structural Safety 2007;29:183–93. doi:10.1016/j.strusafe.2006.07.008
748 [28] Li DQ, Xiao T, Cao ZJ, Zhou CB, Zhang LM. Enhancement of random finite element
749 method in reliability analysis and risk assessment of soil slopes using Subset Simulation.
750 Landslides 2016;13(2):293–303. doi:10.1007/s10346-015-0569-2
751 [29] Wang Z, Broccardo M, Song J. Hamiltonian Monte Carlo methods for Subset Simulation in
752 reliability analysis. Structural Safety 2019;76:51–67. doi:10.1016/j.strusafe.2018.05.005
753 [30] Duncan JM, Sleep MD. Evaluating reliability in geotechnical engineering. In: Phoon K-K,
754 Ching J, editors. Risk Reliab. Geotech. Eng., CRC Press; 2015, p. 50.
755 [31] Schweiger HF, Thurner R, Pöttler R. Reliability Analysis in Geotechnics with Deterministic
756 Finite Elements. Int J Geomech 2001;1:389–413. Doi:10.1061/(ASCE)1532-
757 3641(2001)1:4(389)
758 [32] Sekhavatian A, Janalizadeh Choobbasti A. Comparison of Point Estimate and Monte Carlo
759 probabilistic methods in stability analysis of a deep excavation. International Journal of Geo-

760 Engineering 2018;9(1):20. doi:10.1186/s40703-018-0089-8
761 [33] Liyama K, Yoshiyuki A, Fujita K, Ichimura T, Morikawa H, Hori M. A point-estimate based
762 method for soil amplification estimation using high resolution model under uncertainty of
763 stratum boundary geometry. Soil Dynamics and Earthquake Engineering 2019;121:480-90.
764 [34] Rosenblueth E. Point estimates for probability moments. Proc Natl Acad Sci U S A
765 1975;72:3812–4. doi:10.1073/pnas.72.10.3812.
766 [35] Lind NC. Modelling of uncertainty in discrete dynamical systems. Appl Math Model
767 1983;7:146–52. doi:10.1016/0307-904X(83)90001-X.
768 [36] Harr ME. Probabilistic estimates for multivariate analyses. Appl Math Model 1989;13:313–
769 8. doi:10.1016/0307-904X(89)90075-9.
770 [37] Panchalingam G, Harr ME. Modelling of many correlated and skewed random variables.
771 Appl Math Model 1994;18:635–40. doi:10.1016/0307-904X(94)90322-0.
772 [38] Robertson PK. Interpretation of cone penetration tests — a unified approach. Can Geotech J
773 2009;46:1337–55. doi:10.1139/T09-065.
774 [39] Tonni L, Gottardi G. Interpretation of piezocone tests in Venetian silty soils and the issue of
775 partial drainage. In: Deep foundations and geotechnical in situ testing, ASCE Geotechnical
776 Special Publication No. 178. Reston (Virginia): ASCE; 2010. pp. 367-74.
777 [40] Tonni L, Gottardi G, Amoroso S, Bardotti R, Bonzi L, Chiaradonna A, D'Onofrio A,
778 Fioravante V, Ghinelli A, Giretti D, Lanzo G, Madiai C, Marchi M, Martelli L, Monaco P,
779 Porcino D, Razzano R, Rosselli S, Severi P, Silvestri F, Simeoni L, Vannucchi G, Aversa S.
780 Interpreting the deformation phenomena triggered by the 2012 Emilia seismic sequence on
781 the Canale Diversivo di Burana banks. Rivista Italiana di Geotecnica 2015;49(2):28-58.
782 [41] Kulhawy FH, Mayne PW. Manual on Estimating Soil Properties for Foundation Design.
783 1990.
784 [42] Mayne PW, Campanella RG. Versatile site characterization by seismic piezocone. 16th Int.
785 Conf. Soil Mech. Geotech. Eng. 12-16 Sept. 2005, Osaka, Japan: 2005, p. 721–4.

786 [43] Ouyang Z, Mayne PW. Effective friction angle of clays and silts from piezocone penetration
787 tests. Canadian Geotechnical Journal 2018;55:1230–47 doi:10.1139/cgj-2017-0451
788 [44] Gottardi G, Marchi M, Tonni L. Static stability of Po river banks on a wide area. In: Proc.
789 16th ECSMGE, 2015. p. 1675-80. doi:10.1680/ecsmge.60678
790 [45] Phoon K-K, Kulhawy FH. Characterization of geotechnical variability. Canadian
791 Geotechnical Journal 1999;36:612–624.
792 [46] Ching J, Lin G-H, Chen J-R, Phoon K-K. Transformation models for effective friction angle
793 and relative density calibrated based on generic database of coarse-grained soils. Canadian
794 Geotechnical Journal 2017;54: 481–501. doi:10.1139/cgj-2016-0318
795 [47] Romano N, Santini A. Determining soil hydraulic functions from evaporation experiments by
796 a parameter estimation approach: Experimental verifications and numerical studies. Water
797 Resour Res 1999;35:3343–59. doi:10.1029/1999WR900155.
798 [48] van Genuchten MT. A Closed-form Equation for Predicting the Hydraulic Conductivity of
799 Unsaturated Soils1. Soil Sci Soc Am J 1980;44:892.
800 [49] Olivella S, Gens A. Vapour transport in low permeability unsaturated soils with capillary
801 effects. Transp Porous Media 2000;40:219–41. doi:10.1023/A:1006749505937.
802 [50] Mualem Y. A new model for predicting the hydraulic conductivity of unsaturated porous
803 media. Water Resour Res 1976;12:513–22. doi:10.1029/wr012i003p00513.
804 [51] Schaap MG, Leij FJ, Van Genuchten MT. Neural network analysis for hierarchical prediction
805 of soil hydraulic properties. Soil Sci Soc Am J 1998;62:847–55.
806 [52] Likos WJ, Lu N, Godt JW. Hysteresis and Uncertainty in Soil Water-Retention Curve
807 Parameters. J Geotech Geoenvironmental Eng 2014;140:04013050.
808 [53] Santoso A, Phoon KK, Quek ST. Probability models for SWCC and hydraulic conductivity.
809 In: Proceedings 14th Asian Regional Conference on Soil Mechanics and Geotechnical
810 Engineering, Hong Kong, China, 23-27 May 2011.
811 [54] Robertson PK, Cabal KL. Guide to cone penetration testing for geotechnical engineering. In:

812 Gregg Drilling & Testing I, editor. 6th Edition, 2015, p. 133.
813 [55] Casagli N, Rinaldi M, Gargini A, Curini A. Pore water pressure and streambank stability:
814 Results from a monitoring site on the Sieve River, Italy. Earth Surf Process Landforms
815 1999;24:1095–114.
816 [56] Calabresi G, Colleselli F, Danese D, Giani G, Mancuso C, Montrasio L, et al. Research study
817 of the hydraulic behaviour of the Po River embankments. Can Geotech J 2013;50:947–60.
818 [57] Gragnano CG, Bertolini I, Rocchi I, Gottardi G. On the stability of a fully instrumented river
819 embankment under transient conditions. In: Proceedings CNRIG 2019;40:369-378.
820 [58] Sleep MD, Duncan JM. Effects of initial conditions on the results of transient seepage
821 analyses. In: ASCE, editor. Proc. Geo-Congress 2013 Stab. Perform. Slopes Embankments
822 III, San Diego, California, US: 2013, p. 1081–91.
823 [59] GEO-SLOPE International Ltd. Seepage Modeling with SEEP/W; 2007. http://www.geo-
824 slope.com.
825 [60] GEO-SLOPE International Ltd. Stability modeling with SLOPE/W; 2007. http://www.geo-
826 slope.com.
827 [61] Morgenstern NR, Price VE. Analysis of the stability of general slip surfaces. Géotechnique
828 1965;15(1):79–93.
829 [62] Vanapalli SK, Fredlund DG, Pufahl DE, Clifton AW. Model for the prediction of shear
830 strength with respect to soil suction. Can Geotech J 1996;33:379–92. doi:10.1139/t96-060.
831 [63] Fredlund DG, Morgenstern NR, Widger RA. The shear strength of unsaturated soils. Can
832 Geotech J 1978;15:313–21. doi:10.1139/t78-029.
833 [64] Fredlund DG, Vanapalli SK. Shear strength of unsaturated soils. Agron Soil Test Man
834 2002:329–61.
835 [65] Lu N, Likos WJ. Unsaturated soil mechanics. New York: Wiley. 2004.
836 [66] Gottardi G, Gragnano CG. On the role of partially saturated soil strength in the stability
837 analysis of a river embankment under steady-state and transient seepage conditions. E3S

838 Web Conf., vol. 9, 2016. doi:10.1051/e3sconf/20160919002.
839 [67] Vannucchi G. Analisi probabilistica speditiva in geotecnica e fondazioni. Riv Ital Di Geotec
840 1985;19:77–87.
841 [68] Zhang L, Zhang L, Tang W. Importance of considering correlations among parameters of
842 soil-water characteristic curve. 9th Int. Conf. Appl. Stat. Probab. Civ. Eng., San Francisco,
843 US: 2003, p. 1423–9.
844 [69] Zhang L, Deng H, Zhang L. Reliability analysis of slope stability considering correlations
845 among soil hydraulic parameters. J Shenzhen Univ Sci Eng 2010;27:114–9.
846 [70] Lee I, White W, Ingles O. Geotechnical engineering. Boston, US: Pitman Publishing; 1983.
847 [71] Lacasse S, Nadim F. Uncertainties in characterising soil properties. Publ - Norges Geotek
848 Inst 1996;201:49–75.
849

Figure

**Figure 1** – Images of the breached area during the River Secchia flooding in January 2014.

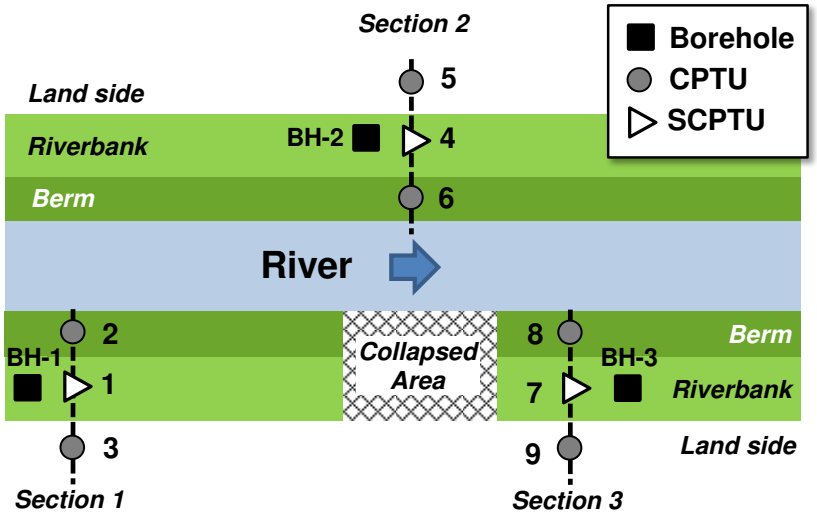


**Figure 2 -** Sketch of the investigated area with location of piezocone tests and boreholes.

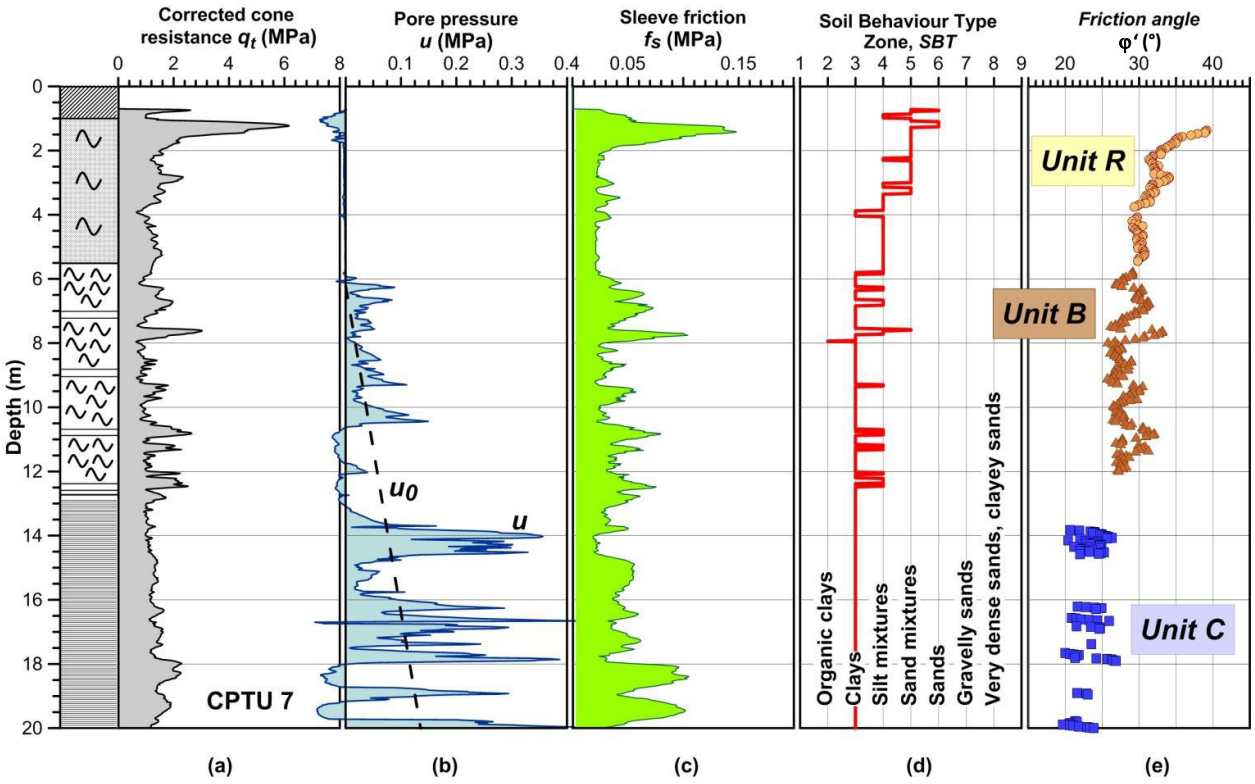


**Figure 3** - SCPTU 7 log profiles and CPTU-based soil classification.

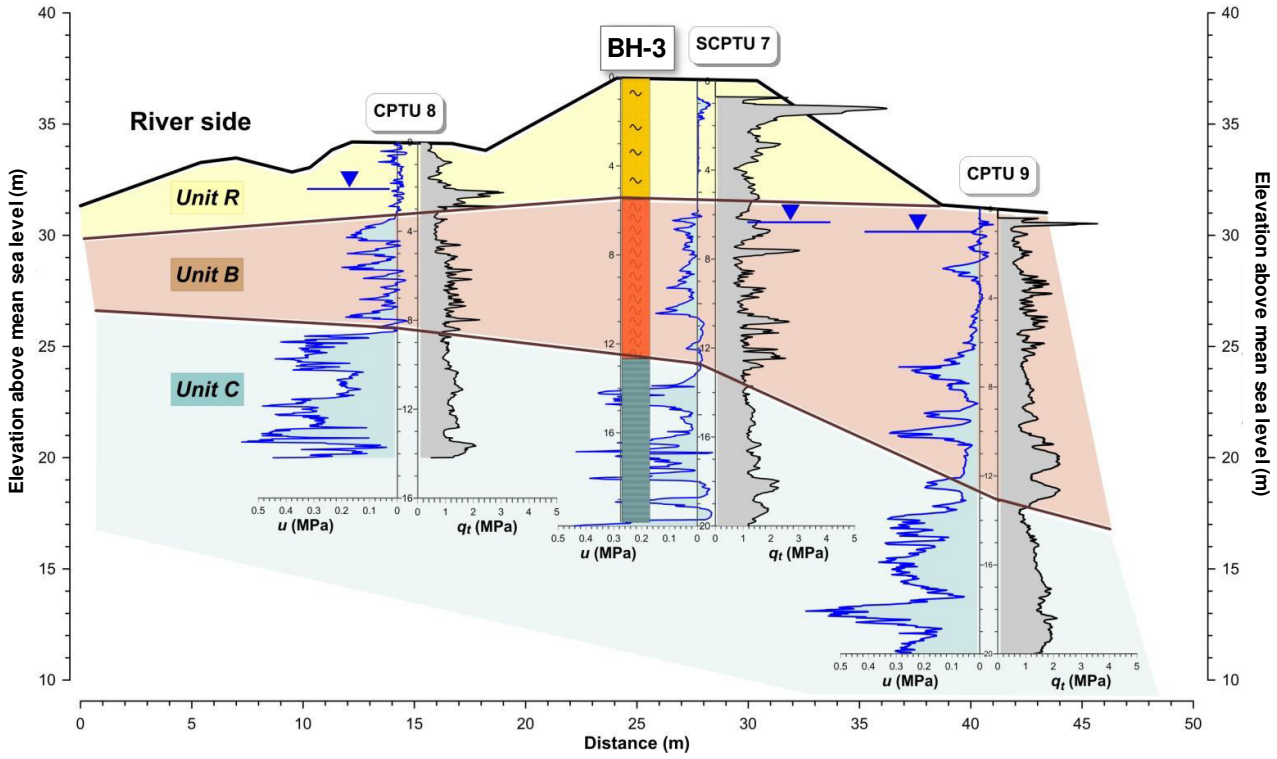


**Figure 4** - Stratigraphic model along cross-section No. 3.

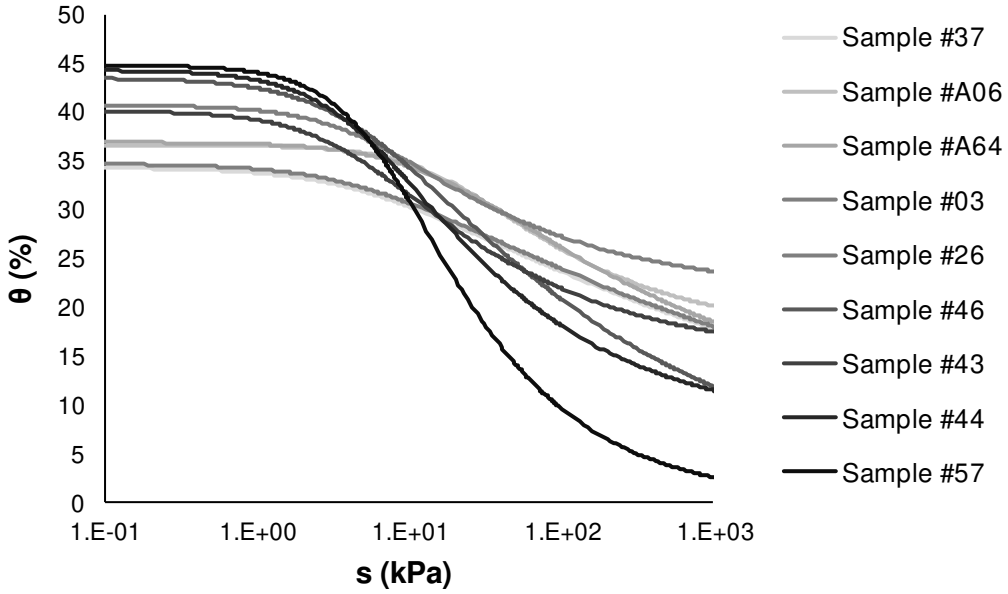


**Figure 5** – Soil water retention curves determined from laboratory experiments.

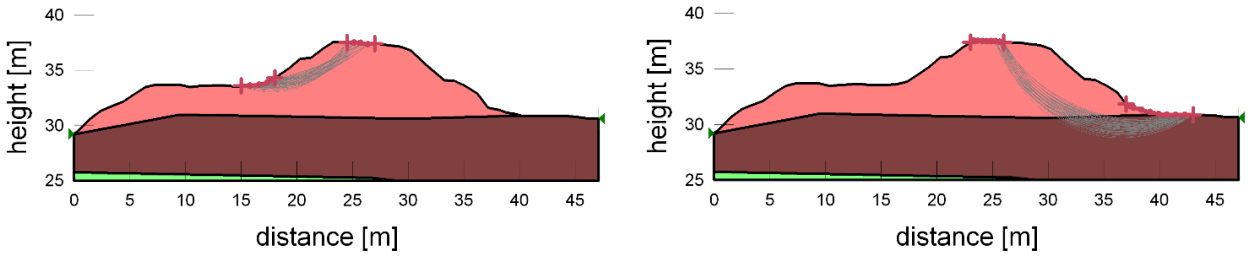


**Figure 6** – Typical slip surfaces investigated in stability analyses for inner (left) and outer (right) slopes.

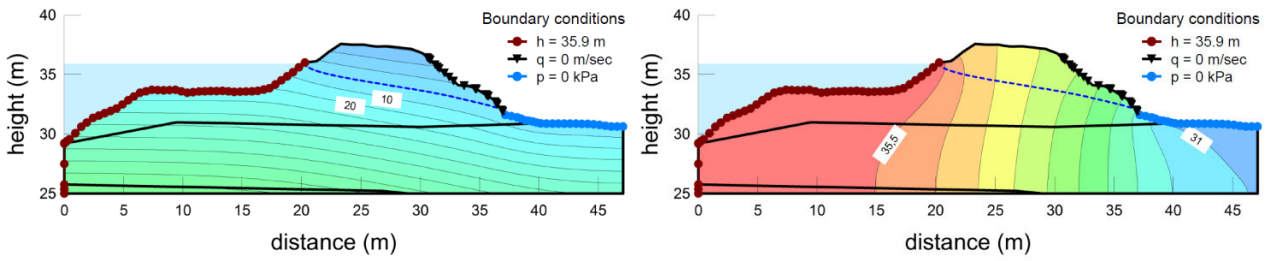


**Figure 7** – Results of the steady state seepage analysis: (left) pore water pressure distribution (isoline increment = 10 kPa) and (right) total head distribution (isoline interval = 0.5 m).

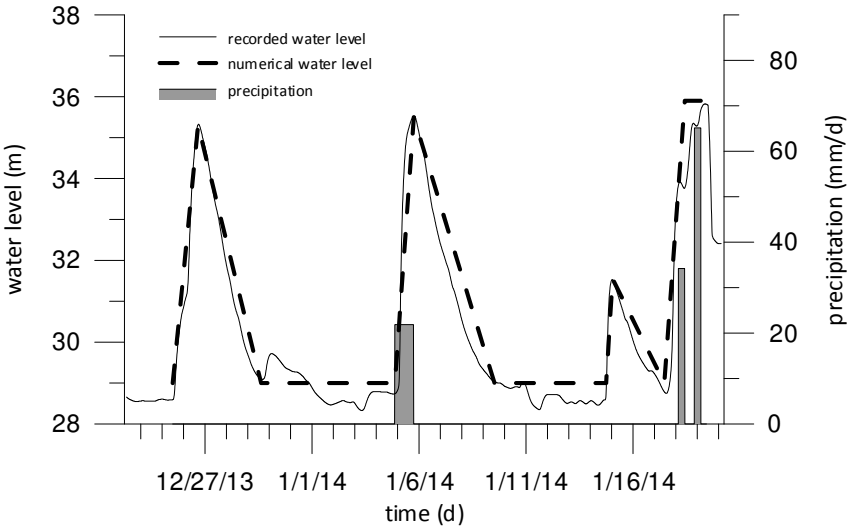


**Figure 8** – Flood hydrograph, rainfall hyetograph and numerical total hydraulic head boundary condition recorded and modelled from 25 December 2013 to 19 January 2014.

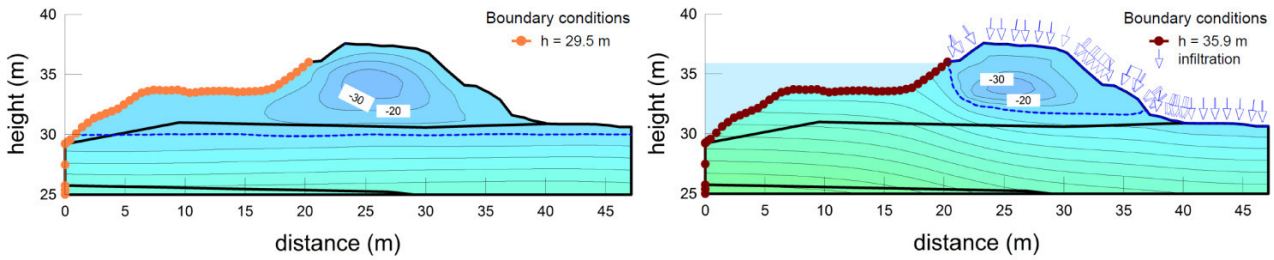


**Figure 9** – Pore water pressure distribution in the initial (left) and final (right) stage of transient seepage analysis (the increment between two adjacent isolines is 10 kPa).

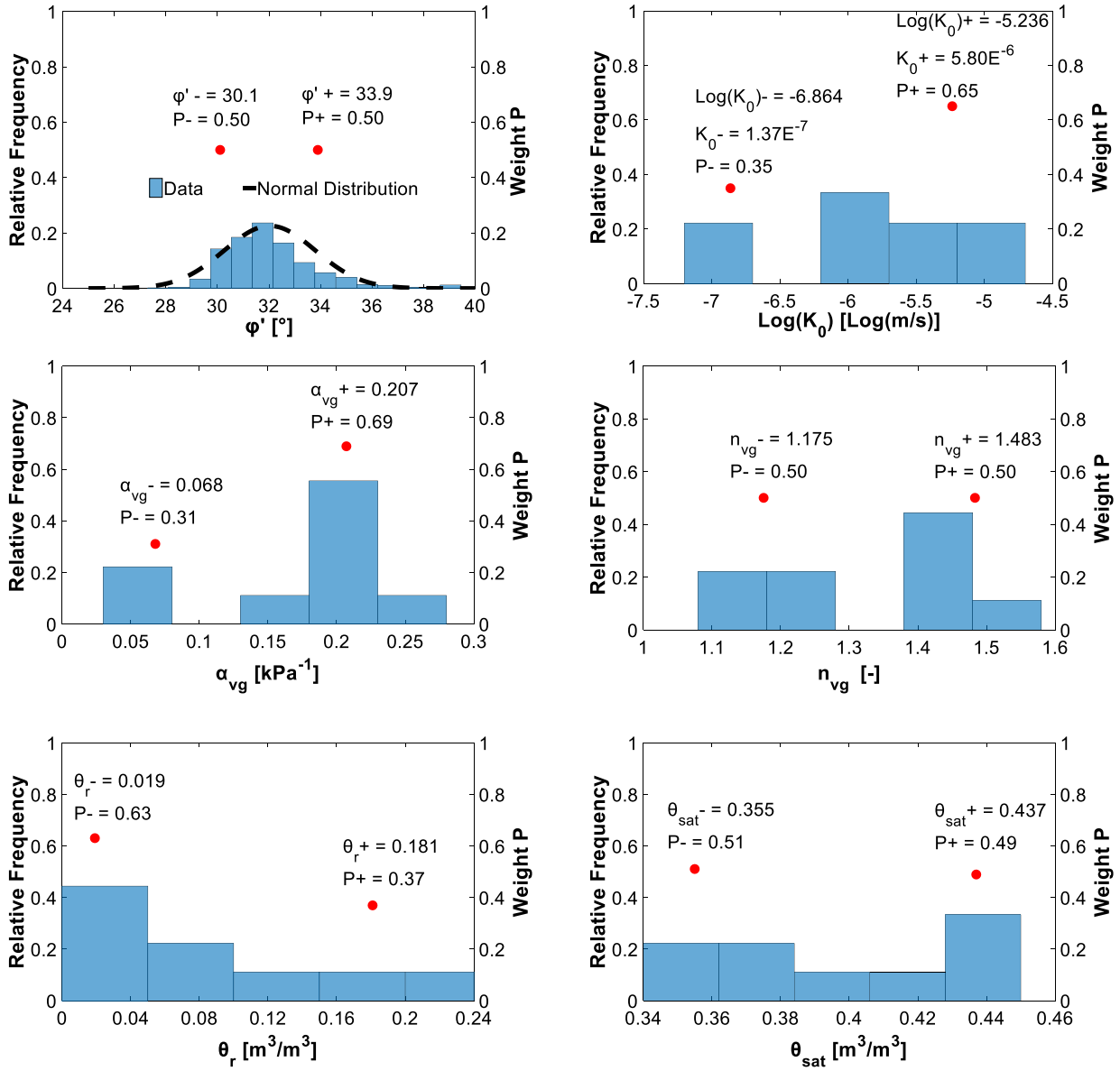


**Figure 10** – Histogram of soil parameters with point estimate locations and relative weights.

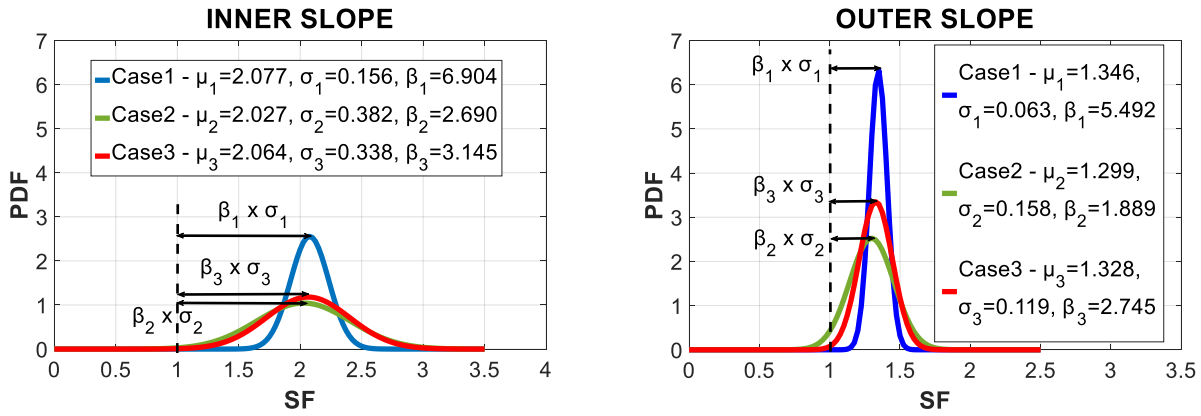


**Figure 11** – Probability density function (PDF) of the safety factor (SF) for both inner slope (left) and outer slope (right), for Case 1, Case 2 and Case 3, including the graphical estimate of the reliability index $\beta$.

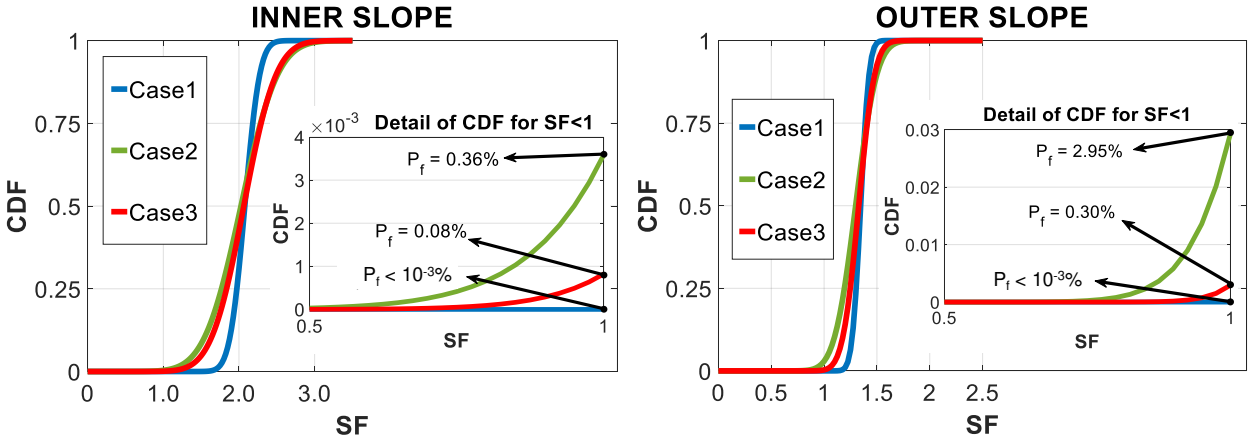


**Figure 12** – Cumulative density function (CDF) of the safety factor (SF) for both inner slope (left) and outer slope (right), for Case 1, Case 2 and Case 3, including the graphical estimate of the probability of failure $P_f$.

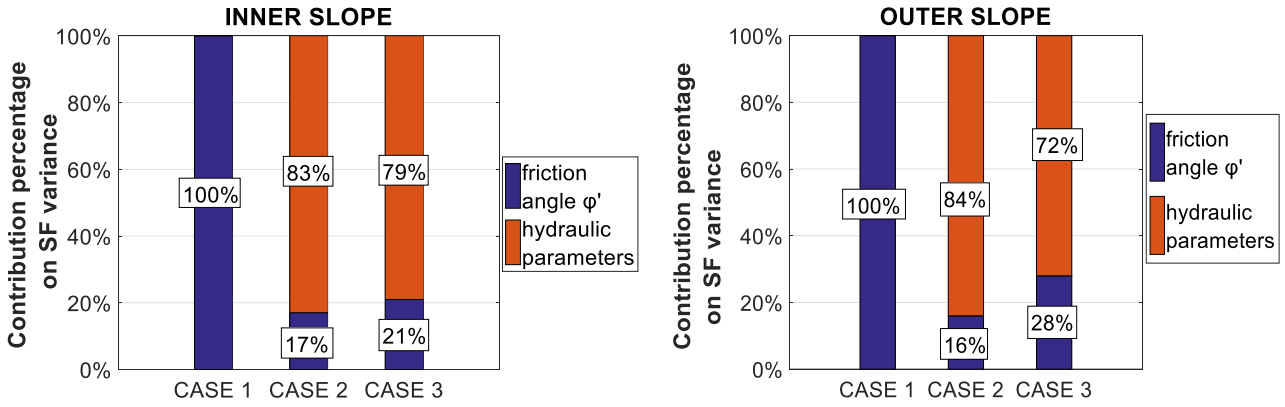


**Figure 13** – Contribution of the hydraulic parameters and shear strength φ' on the safety factor variance, for both inner slope (left) and outer slope (right).

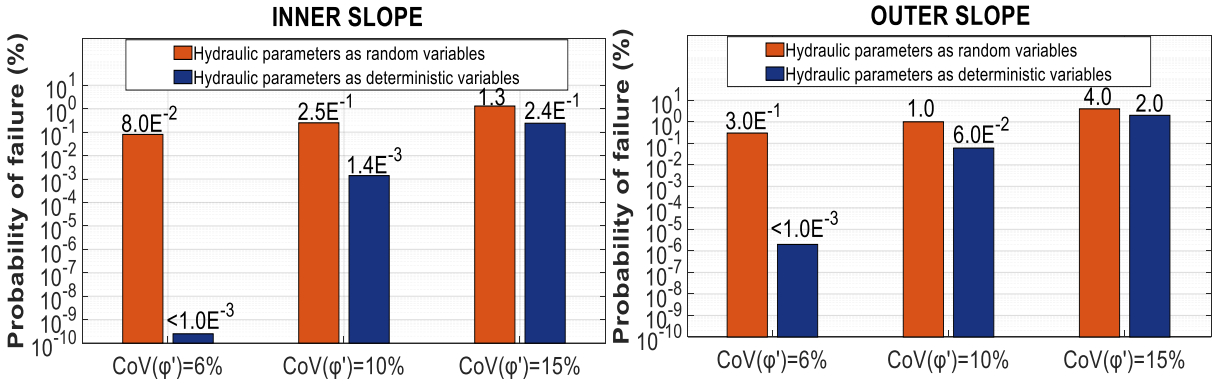


**Figure 14** – Probability of failure vs. coefficient of variation of φ', for both inner slope (left) and outer slope (right), considering the hydraulic parameters as deterministic and as random variables.